European Journal of Medicinal Chemistry Reports 3 (2021) 100011

HOSTED BY

Contents lists available at ScienceDirect

European Journal of Medicinal Chemistry Reports

journal homepage: www.editorialmanager.com/ejmcr/default.aspx

Structure activity relationship of the binding of *p*-coumaroyl glucose to glycogen phosphorylase and its effect on hepatic cell metabolic pathways

Anastasia S. Tsagkarakou [a], Styliani A. Chasapi [b], Symeon M. Koulas [a], Ioannis Tsialtas [a], Efthimios Kyriakis [a], Christina E. Drakou [a], Sándor Kun [c], László Somsák [c], Georgios A. Spyroulias [b,**], Anna-Maria G. Psarra [a,***], Demetres D. Leonidas [a,*]

[a] Department of Biochemistry & Biotechnology, University of Thessaly, Biopolis, 41500, Larissa, Greece
[b] Department of Pharmacy, University of Patras, GR-26504, Greece
[c] Department of Organic Chemistry, University of Debrecen, POB 400, H-4002, Debrecen, Hungary

ARTICLE INFO

Keywords:
Glycogen phosphorylase
Enzyme inhibition
X-ray crystallography
p-Coumaroyl glucose
Glycogen metabolism
NMR metabolomics

ABSTRACT

The binding of *p*-coumaroyl glucose to glycogen phosphorylase (GP; a pharmaceutical target for the development of antihyperglycaemic drugs) has been studied by kinetics, and X-ray crystallography while its effect to HepG2 cells metabolism has been assessed by NMR metabolomics. *p*-Coumaroyl glucose is a potent inhibitor of human liver GP with a K_i value of 213 μM that binds at the active site of the enzyme. Comparative structural analysis with chemically similar GP inhibitors reveals the structural basis of its inhibitory potency. NMR metabolomics analysis revealed that HepG2 cells in the presence of *p*-coumaroyl glucose actively response to higher glucose uptake from their environment and a display an ''insulin-sensitizing'' state. Furthermore, NMR metabolomics analysis indicates an enhancement of gluconeogenesis towards lipid metabolism and glycerol-derived components.

1. Introduction

Glycogen phosphorylase (GP; EC 2.4.1.1) is the key enzyme of glycogen metabolism, catalyzing the phosphorolysis of the α-1,4 glycosidic bonds of glycogen to yield glucose-1-phosphate [1,2]. Since glycogen metabolism is a key metabolic process for glucose homeostasis, GP has been the focus of many inhibition studies for the development of novel agents to treat hyperglycemia in the context of type 2 diabetes (T2D). Over the last decade GP cellular and animal studies have shown that GP inhibition leads to a better hepatic glycogen balance and blood glucose levels control [3]. These results are also supported by *in vitro*, *ex vivo* and *in vivo* studies [1,2,4–8]. It has been also suggested that GP inhibitors can also target pancreatic cells and hence they can improve *β*-cell function and survival [9]. Moreover, GP inhibition is now recognized to have a significant potential for the treatment of other conditions such as cancer, myocardial and cerebral ischemias [10–12]. In a very recent study, it has been pointed out that some glucose derived GP inhibitors act also on sodium dependent glucose cotransporters (SGLTs), another target in combatting T2D with marketed drugs called gliflozins [13]. This will further enhance the value of GP inhibitors as potential pharmaceuticals.

GP is an allosteric enzyme that balances between two major conformation states, a T state with low activity and affinity for substrates and an R state with high activity and affinity for substrates [4]. The biologically active GP is a dimer, with a cofactor pyridoxal 5′-phosphate (PLP) molecule and it is regulated allosterically by phosphorylation. It therefore exists in two interconvertible forms: GPa is the Ser14 phosphorylated form (R state); GPb is the unphosphorylated form (T state). X-ray crystallography and enzyme kinetics have identified seven distinct ligand binding sites in GP: the active, the inhibitor, the allosteric, the glycogen storage, the indole binding, the quercetin, and the benzimidazole binding sites [14]. The conformational changes responsible for GP conversion from its inactive T to its active R state by phosphorylation or ligand-binding at the allosteric site [15,16] are mainly focused in a flexible loop (280s loop; residues 280–286) which controls entrance to a long channel that leads to the active site. Potent GP inhibitors with K_i values in the range of low μM to nM stabilize the obstructing conformation of the 280s loop locking thus the enzyme in the inactive T state conformation.

* Corresponding author. Department of Biochemistry and Biotechnology, University of Thessaly, Biopolis, 41500, Larissa, Greece.
** Corresponding author.
*** Corresponding author. Department of Biochemistry and Biotechnology, University of Thessaly, Biopolis, 41500, Larissa, Greece.
E-mail addresses: G.A.Spyroulias@upatras.gr (G.A. Spyroulias), ampsarra@bio.uth.gr (A.-M.G. Psarra), ddleonidas@bio.uth.gr (D.D. Leonidas).

https://doi.org/10.1016/j.ejmcr.2021.100011
Received 24 August 2021; Received in revised form 4 October 2021; Accepted 17 October 2021
Available online 27 October 2021

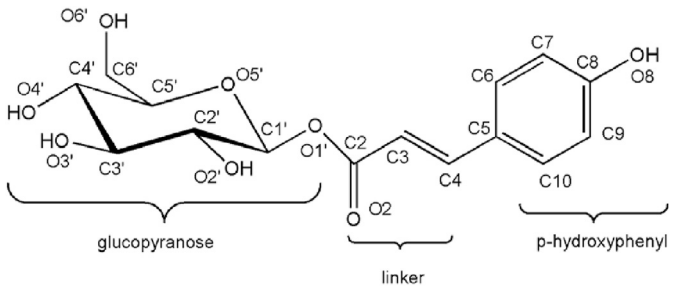

Scheme 1. The chemical structure of *p*-coumaroyl glucose (1-*O*-(4-coumaroyl)-*β*-D-glucose) with the crystallographic numbering.

In recent years, several studies have explored phytogenic compounds, extracts, and mixtures in a quest to discover new potent GP inhibitors [1,14,17–19]. This has led to the discovery of some strong inhibitors such as ellagic ($K_i = 13.4$ μM) [17], and asiatic acid ($IC_{50} = 17.0$ μM) [20], some iminosugars like 1,4-dideoxy-1,4-imino-D-arabinitol ($IC_{50} = 0.39$ μM) [21], and chrysin ($K_i = 19.0$ μM) [22]. Although, phytogenic polyphenols and especially triterpenes and flavonoids have been found to be potent inhibitors of GP [1], little is known on the effect of soluble phytogenic compounds. *p*-Coumaric acid (*p*-CA), a phenolic acid of the hydroxycinnamic acid family, in free or bound form is found in fruits, vegetables, cereals, herbs, and mushrooms [23]. *p*-CA and its conjugates have been shown to act as moderators of hyperglycemia by inhibiting α-glucosidase [24], aldose reductase [25,26], the processes of gluconeogenesis and adipogenesis [23], by activating AMP-activated protein kinase [27], and by increasing insulin sensitivity reducing post-prandial hyperglycemia [23]. However, the effect of *p*-CA conjugates on the GP activity has not been studied yet. A water soluble conjugate of *p*-CA, *p*-coumaroyl-glucose (1-*O*-(4-hydroxycinnamoyl)-β-D-glucopyranose; Scheme 1) is present in a variety of herbal teas. A study of chamomile tea and its individual components showed a significant effect on lowering blood glucose levels *in vitro* and in streptozotocin (STZ)-induced diabetic rats [28]. Other studies showed that consumption of chamomile tea has some beneficial effects on glycemic control in T2D patients [29,30]. Furthermore, chamomile tea has been shown to inhibit digestive enzymes (α-amylase and maltase) related to intestinal sugar release [31]. To investigate the bioactivity of *p*-coumaroyl glucose against GP we have performed a kinetic and X-ray crystallography study on the binding of *p*-coumaroyl glucose to GP. Furthermore, we studied the effect of *p*-coumaroyl glucose on the metabolome of HepG2 cells. Our results show that *p*-coumaroyl glucose is a potent inhibitor of GP with a significant effect on the metabolism of HepG2 cells. This is the first time that a GP inhibitor has been shown to affect the metabolic pathways at cellular level and as such the analysis will have significant impact on future antihyperglycaemic drug discovery studies targeting GP.

2. Materials and methods

2.1. Synthesis

2.1.1. General methods

Melting points were measured on a Kofler hot-stage and the values are uncorrected. NMR spectra were recorded on Bruker DRX360 (360/90 MHz for $^1H/^{13}C$) and DRX400 (400/100 MHz for $^1H/^{13}C$) spectrometers. Chemical shifts are referenced to internal Me_4Si (^1H) or the residual solvent signals (^{13}C). Mass spectra were recorded using a Thermo LTQ XL mass spectrometer (Thermo Electron Corp., San Jose, CA, USA) using positive-ion ESI mode. Thin-layer chromatography (TLC) was carried out on aluminium sheets coated with Silica Gel 60 F254 (Merck). Silica gel column chromatography was performed with Kieselgel 60 (particle size 63–200 μm; Molar Chemicals). 2,3,4,6-Tetra-*O*-chloroacetyl-D-glucopyranosyltrichloroacetimidate (**1**) was prepared by a literature method [32].

3. 4-Chloroacetoxycinnamic acid (2)

To the solution of *p*-coumaric acid (**4**, 2 g, 12.2 mmol) and triethylamine (6.8 mL, 48.7 mmol, 4 equiv.) in anhydrous THF (40 mL) chloroacetyl chloride (1.94 mL, 24.4 mmol, 2 equiv. in 4 mL of anhydrous THF) was added dropwise at 0 °C. After 4 h of stirring the mixture was poured into ethyl acetate (50 mL) and extracted with 1 M aqueous HCl (30 mL) and brine. The organic phase was dried over $MgSO_4$, filtrated, and concentrated under reduced pressure. The resulting crude product was purified by column chromatography (toluene-acetic acid 19:1 → 9:1 gradient) to yield 2.6 g (89%) of white crystalline product. m.p. 183–185 °C (lit. m.p. 186–187 °C [33]). $R_f = 0.55$ (toluene-acetic acid 4:1) ^1H NMR (400 MHz, DMSO-d_6): 12.44 (1H, s, COO*H*); 7.78 (2H, d, $J = 8.6$ Hz, Ar), 7.61 (1H, d, $J = 16.0$ Hz, Ar-C*H*═CH-); 7.24 (2H, d, $J = 8.6$ Hz, Ar); 6.53 (1H, d, $J = 16.0$ Hz, Ar-CH═C*H*-); 4.71 (2H, s, CO*CH*$_2$Cl); ^{13}C NMR (100 MHz, DMSO-d_6): 167.4, 166.2 (*C*═O); 151.4, 142.8, 132.4, 129.6, 122.0, 119.6 (Ar, -*C*H =), 41.3 (-CO*C*H$_2$Cl).

4. 2,3,4,6-Tetra-*O*-chloroacetyl-*l*-*O*-(4-chloroacetoxycinnamoyl)-β-D-glucopyranose (3)

Compound **3** was prepared according to the published procedure [34].

5. *l*-*O*-(4-hydroxycinnamoyl)-β-D-glucopyranose (5)

Compound **3** (50 mg, 0.07 mmol) was dissolved in a 1:1 mixture of anhydrous methanol and chloroform (2 mL) and triethylamine (50 μL, 0.35 mmol) was added at 0 °C. After 2 h of stirring at this temperature the volatiles were removed under reduced pressure and the residue was purified by column chromatography (eluent: chloroform-methanol 9:1 → 4:1 gradient) to give 19 mg (83%) colourless syrup. $R_f = 0.28$ (chloroform-methanol 4:1). ^1H and ^{13}C NMR spectra are in good agreement with those reported in methanol-*d4* solvent [34,35]. ^1H NMR (360 MHz, DMSO-d_6): 7.63 (1H, d, $J = 15.9$ Hz, Ar-C*H*═CH-), 7.56 (1H, d, $J = 8.6$ Hz, Ar), 6.81 (1H, d, $J = 8.6$ Hz, Ar), 6.37 (1H, d, $J = 15.9$ Hz, Ar-CH═C*H*-), 5.44 (1H, d, $J = 7.9$ Hz, H-1), 3.44 (1H, dd, $J = 12.1$, 5.4 Hz, H-6), 3.28–3.10 (5H, m, H-2, H-3, H-4, H-5, H-6'); ^{13}C NMR (90 MHz, DMSO-d_6): 165.8 (*C*═O), 160.2, 146.4, 130.9, 125.3, 116.1, 113.9 (Ar, -*C*H =), 94.5 (C-1), 77.9, 76.5, 72.6, 69.7 (C-2 – C-5), 60.8 (C-6). ESI-MS: Calculated $[M+Na]^+$: 349.09, Found: 349.17.

5.1. Enzyme kinetics

Rabbit muscle and human liver GPa (rmGPa and hlGPa) were produced following previously established protocols [36]. Enzymatic activity was measured in the direction of glycogen synthesis following a procedure described earlier [37]. Initial velocities were calculated from the pseudo-first order rate constants using the first-order rate equation and inhibition constant (*K*i) values were calculated from the plot of *K*m(app.) vs [inhibitor] using the non-linear regression program GRAFIT [38] and an explicit weighting.

5.2. X-ray crystallography

T state rabbit muscle GPb (rmGPb) crystals were grown as described previously [37]. Ligand complexes were produced by soaking preformed rmGPb crystals in a solution of 10 mM *p*-coumaroyl glucose in the crystallization media supplemented with 10% (v/v) DMSO 24 for h at room temperature. X-ray diffraction data were collected using synchrotron radiation at beamline P13 of the EMBL-Hamburg outstation at room temperature on a Pilatus 6 M detector. Crystal orientation, integration of reflections, inter-frame scaling, partial reflection summation, and data reduction was performed by the program XDS [39] while scaling and merging of intensities, was performed by Aimless [40]. Crystallographic refinement of the complexes was performed by maximum-likelihood

Table 1
Summary of the diffraction data processing and refinement statistics for the GPb - *p*-coumaroyl glucose complex. Values in parentheses are for the outermost shell.

Data Processing and collection statistics	
Space group and unit cell dimensions	$P4_32_12$, a = b = 128.6 Å, c = 116.6 Å
Resolution (Å)	1.60 (1.63–1.60)
Reflections measured	835324 (36085)
Unique reflections	128346 (6280)
R_{merge}	0.046 (0.621)
Completeness (%)	99.9 (99.9)
$< I/\sigma(I) >$	15.1 (3.0)
Multiplicity	6.5 (5.7)
$CC^{1/2}$	0.998 (0.900)
B Wilson ($Å^2$)	28.2
Reflections used for refinement	114728 (8739)
No of water molecules	451
No of ligand atoms	23
R (%)	12.8 (16.1)
R_{free} (%)	32.0 (35.5)
r.m.s.d. in bond lengths (Å)	0.007
r.m.s.d. in bond angles (°)	1.2
Average B ($Å^2$)	
Protein atoms	36.4
Water molecules	48.9
Ligand atoms	29.8
PDB entry	7ONF

methods using REFMAC [41] using as starting model the structure of the free T state rmGPb (pdb entry 7P7D [42]). Ligand molecule coordinates and topologies were constructed using JLigand [43] and they were fitted to the electron density maps by adjusting of their torsion angles. A summary of the data processing and refinement statistics for the inhibitor complex structure is given in Table 1. The validity of the refinement procedure was checked using the PDB_REDO server [44]. As there were more than 5 reflections per atom available, both an isotropic and an anisotropic B-factor model were considered, and the anisotropic B-factor model was selected based on the Hamilton R ratio test. A TLS model for grouped atom movement with one TLS group was used. The stereochemistry of the protein residues was validated by MolProbity [45]. Hydrogen bonds and van der Waals interactions were calculated with the program CONTACT as implemented in CCP4 [46] applying a distance cut off 3.4 Å and 4.0 Å, respectively. Accessible surfaces were calculate using NACCESS [47]. Figures were prepared with CCP4 Molecular Graphics [48]. The coordinates of the new structure have been deposited with the RCSB Protein Data Bank (http://www.rcsb.org/pdb) with code presented in Table 1.

5.3. Cellular studies

For the assessment of the effect of *p*-coumaroyl glucose on the hepatocarcinoma HepG2 cells metabolic profile, human HepG2 hepatocarcinoma cells that were maintained in Dulbecco's modified Eagle medium (DMEM), containing 25 mM glucose 10% FBS, 2 mM glutamine, and penicillin/streptomycin, in a humidified atmosphere with 5% CO2, at 37 °C, were seeded in 60 mm culture dishes at a density of 1.5×10^6 cells per dish. After cell attachment (16–18 h), the medium was replaced by serum-free medium containing 10 nM dexamethasone, 25 mM glucose, and 100 nM insulin, and cells were further incubated for 16–18 h to replete glycogen stores [18]. Cells were then incubated in the presence or absence of 400 μM *p*-coumaroyl glucose in serum- and glucose-free medium supplemented with 100 nM glucagon for 3 h. Subsequently, growth media were collected, and cells were washed in phosphate buffer, harvested, and centrifuged at 700 g for 5 min. Cell pellets were resuspended in lysis buffer containing 20 mM Tris pH 7.5, 0.5% (v/v) Triton X-100, 250 mM NaCl και 3 mM EDTA, supplemented with 1 mM DTT, 0.1 mM PMSF and cocktail inhibitors (Roche). Extracellular growth media as well as cell lysates were subjected to NMR analysis.

5.4. NMR metabolomics

NMR samples were prepared by mixing 70 μL of cell extract with 530 μL of 1.5 M potassium phosphate buffer (pH 7.4) to a final volume of 600 μL. Samples contained 100% D2O (v/) and 0.1 mM DSS, used as internal standard chemical shift reference. For control experiments 300 μL of cell media mixed with 300 μL of potassium phosphate buffer (pH 7.4, 100% D2O (v/v) and 0.1 mM DSS). Samples were vortexed briefly and transferred in a 5-mm NMR tube (Bruker BioSpin srl.) for analysis.

The ^{1}H NMR spectra were recorded at 298 K on a Bruker Avance III HD 700 MHz NMR spectrometer equipped with a cryogenically cooled 5.0-mm ^{1}H/^{13}C/^{15}N/D Z-gradient probe. For each sample, three ^{1}H NMR spectra were acquired. A mono-dimensional (1D) NMR spectrum acquired using a standard Carr-Purcell-Meiboom-Gill (cpmgpr1d.comp; Bruker BioSpin) pulse sequence was applied to remove the broad signal contribution from proteins and other high-molecular-weight components imposing a T_2 filter. All monodimensional spectra were acquired with 128 scans, a relaxation time of 4 s, receiver gain of 50.8, 128 scans and a spectral width of 19.9993 ppm. Additional, ^{1}H–^{1}H *J*-resolved (jresgpprqf.comp; Bruker BioSpin) pulse sequence was performed in order to facilitate metabolite identification separating chemical shifts and *J*-couplings into two different spectral dimensions. Two dimensional ^{1}H–^{13}C HSQC nmr spectrum helped in the accurate assignment and specially of highly overlapping spectral regions present in all the monodimensional spectra. For all samples matching and shimming performed manually.

Free induction decays were multiplied by an exponential function equivalent to a 1.0 Hz line-broadening factor before applying Fourier transform. Transformed NMR spectra were phased, baseline-corrected and calibrated (using as a reference peak the 1H signal of the anomeric hydrogen of a-glucose doublet at 5.24 ppm) manually using Topspin 3.2 (Bruker BioSpin srl). Each processed NOESY spectrum (0.06–9.00 ppm) was uniformly segmented into 0.02 ppm spectral width buckets in Amix 3.9.13 software (Bruker Biospin). Spectral regions between 5.20 and 4.18 ppm containing residual water reducing the system to 406 bins. The resulting data sets were separately imported into MetaboAnalyst 5.0 software [49] for statistical analysis and evaluation.

NMR data analysis followed by an untargeted analytical approach. A variety of multivariate and univariate statistical methods applied on the obtained bucket files. The original NMR data were subjected to both unsupervised and supervised methods. All NMR spectra subjected into Principal component analysis (PCA) to identify any clustering trends and control the datasets for the presence of outliers. Additionally, Partial least squares discriminant analysis (PLS-DA) was performed as a supervised method of classification. Bucket tables resulting from the 1D NOESY spectra were used to construct the subsequent classification models. For the assessment of the class discrimination and the prediction ability of the classification models' standard definitions were used.

To examine the detailed relationships between the concentrations of the top 30 metabolites/variables resulted from ANOVA in the 12 samples, correlation heatmaps were ordered according to hierarchical clustering, Ward linkage. Pearson's correlation coefficient was used to reveal the kind of correlation between each pair. Metabolite identifications were performed using Chenomx NMR software (Profiler 8.1 Chenomx Inc., Canada), the public database (HMDB) and literature data.

6. Results & discussion

6.1. Synthesis

The first synthesis of *p*-coumaroyl-β-D-glucopyranose (**5**) was achieved by the biotransformation of *p*-coumaric acid (**4**) or cinnamic acid using the cultured cells of the *Eucalyptus perriniana* [50]. Chemical synthesis of **5** was carried out by the glycosylation of *O*-chloroacetyl protected *p*-coumaric acid **2** with trichloroacetimidate **1** followed by

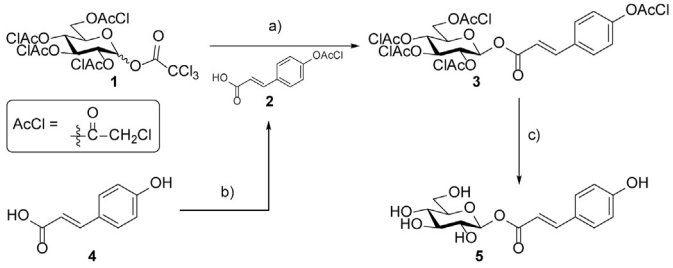

Scheme 2. The synthesis of *p*-coumaroyl glucose. Reagents and conditions: a) TMSOTf, anh. DCM, 4 Å MS, 0 °C, 28%; b) $ClCH_2COCl$, Et_3N, anh. THF, 0 °C, 89%; c) Et_3N, anh. MeOH, $CHCl_3$, 0 °C, 83%.

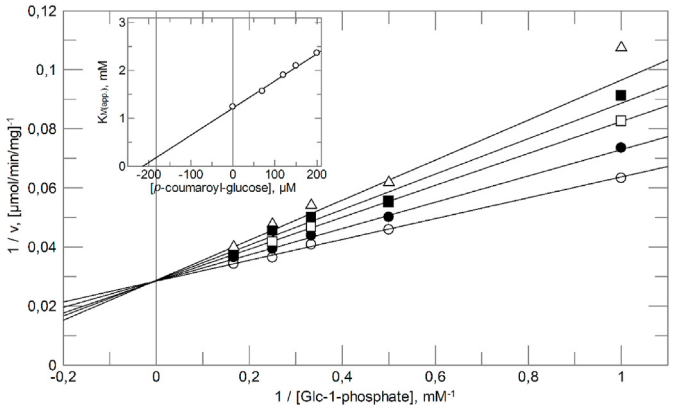

Fig. 1. Competitive inhibition of hlGPa at 0.2% w/v glycogen, different Glc-1-P concentrations (1, 2, 3, 4, and 6 mM) and different inhibitor concentrations (0 (●), 70 (♀), 120 (→), 150 (†), and 200 (➡) μM). The insert plot of the $K_{M(app.)}$ versus inhibitor concentration yields the K_i value.

deprotection to **5** (Scheme 2) [34]. In this study, for the preparation of **5** the published synthetic strategy was applied with minor modifications to obtain compounds **2** [33] and **5** [34] in higher yields as compared to the reported methods. Acylation of *p*-coumaric acid (**1**) with chloroacetyl-chloride in THF resulted in **2** in excellent yield which was then glycosylated by imidate **1** [32] under the published conditions [34] to give glucosyl ester **3**. Mild deprotection of **3** with triethylamine in methanol resulted in *p*-coumaroyl glucose **5** in high yield.

6.2. Enzyme inhibition

The physiological inhibitor of GP, α-D-glucose, displays K_i values of 1.7 2.0 and 4.3 mM for rmGPb [51] rmGPa [52], and hlGPa [53], respectively. *p*-Coumaroyl glucose is a potent, competitive to Glc-1-P, inhibitor of rmGPb ($K_i = 31.4 \pm 1.9$ μM), rmGPa ($K_i = 67.7 \pm 4.2$ μM) and hlGPa ($K_i = 212.9 \pm 12.5$ μM) as revealed by the Lineweaver-Burk plots that intersect at the same point on the y-axis (Fig. 1). As indicated by the K_i values, for all three enzymes, *p*-coumaroyl glucose is more potent for rmGPb than for rmGPa or hlGPa. The difference in the K_i values is significant indicating that this inhibitor can differentiate between the three enzymes. Based on the absolute conservation of the active site of the three enzymes this could imply that *p*-coumaroyl glucose also binds at another binding site of GP (e.g., the AMP or the inhibitor binding site) with different affinity for the three enzymes. However, no binding was found at the crystal at these sites despite the high concentration of *p*-coumaroyl glucose used for soaking GP crystals. We must note here that although it is always better to investigate binding at a site by co-crystallization experiments all six binding sites of rmGPb are solvent accessible and are not occluded by any crystal packing contacts in the tetragonal crystals we used in our experiment. A possible explanation for this preference might be that the R state conformation of

Table 2
Inhibition constants for *p*-coumaroyl glucose and similar inhibitors for rmGPb.

Entry	Inhibitor	K_i (μM)
	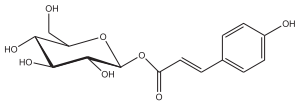	31.4 ± 1.9
1	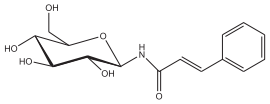	18 [2]
2	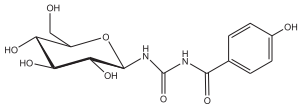	6.3 [2]
3	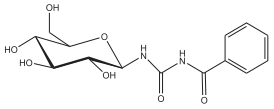	4.6 [56]
4	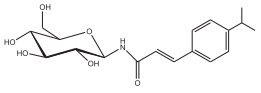	4.98 [54]
5	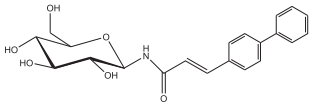	8.25 [54]
6	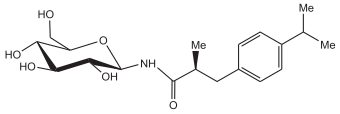	75.3 [54]
7	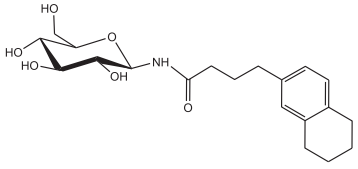	48.7 [54]

the phosphorylated GP isoenzymes (rmGPa and hlGPa) is less sensitive than the R state of the AMP activated rmGPb for *p*-coumaroyl glucose.

In the absence of any inhibitor studies with *O*-acyl-β-D-glucopyranosyl compounds to GP the chemically closest inhibitors to *p*-coumaroyl-glucose are the *N*-acyl-β-D-glucopyranosylamines (entries 2 and 3) and *N*-acetyl-β-D-glucopyranosylamines (entries 1, 4–7) [54,55] presented in Table 2. The inhibitory potency of *p*-coumaroyl-glucose is similar to that of entry 1 but weaker than those of entries 2–5. Nevertheless, is

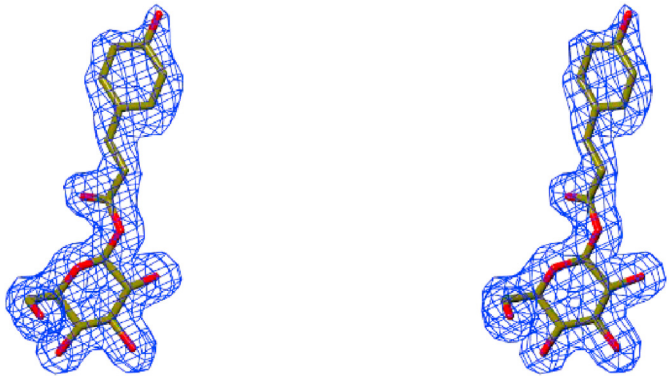

Fig. 2. Stereo diagram of the sigmaA 2Fo-Fc electron density map, contoured at 1 σ, for the bound *p*-coumaroyl glucose at rmGPb. Electron density map was calculated before incorporating the inhibitor molecule in the refinement procedure.

Table 3
Interactions of *p*-coumaroyl glucose with rmGPb residues in the crystal.

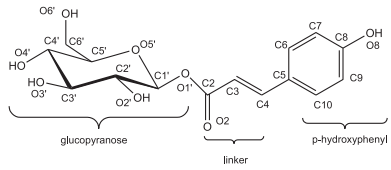

		Hydrogen bonds		Van der Waals interactions
	Inhibitor atom	Protein Residues (atoms)	Distance (Å)	Protein Residues (atoms)
Glucopyranose atoms	O1′			Asn284(CG, ND2, OD1)
				His377(CB, O)
	O2′	Tyr573(OH)	3.1	Asn284(CG, OD1)
		Glu672(OE2)	3.2	
		Asn284(ND2)	2.9	
		Water-219	2.8	
		Water-384	2.8	
	O3′	Ser674(N)	3.0	Ala673(C, CA, CB) Ser674(CA, C)Glu672(CG, CD, C)
		Gly675(N)	3.1	
		Glu672(OE2)	2.7	
		Ala673(N)	3.3	
	O4′	Gly675(N)	2.9	Gly675(C, O, CA) Thr676(N) Ser674(CB, C) Asn484(ND2)
		Water-299	2.7	
	O5′			His377(CD2, CB, CG) Leu136(CB, N)
	O6′	Asn484(ND2)	2.8	His377(CD2, NE2, CG)
				Val455(CG2, CB, CG1)
				Leu139(CD2)
				Asn484(CG)
	C2′			Glu672(OE2) His377(O)
	C3′			Gly675(N) Glu672(OE2)
	C4′			Gly675(N) Water-299
	C5′			Gly135(C) Leu136(N) Water-299
	C6′			Gly135(C, O) His377(CD2) Asn484(ND2) Leu136(CA, N)
Linker atoms	O2	Leu136(N)	3.1	Leu136(CB, CA) Gly135(N) Asn284(ND2) Asp283(OD1)
	C2			Leu136(CB) Asn284(ND2)
	C3			Asn284(CG, ND2, N)
	C4			Leu136(CB, CD1) Asn284(N)
p-hydroxyphenyl atoms	O8	Phe285(O)	3.2	His341(NE2) Arg292(NH2)
	C5			Asn284(N) His341(CE1)
	C6			Asn284(N, CA) His341(CE1, NE2)
	C7			Asn284(N) His341(CE1, NE2) Phe285(N, O)
	C8			Asn282(O) His341(CE1, NE2) Phe285(O)
	C9			Asn282(O) Glu88(OE2) His341(CE1)
	C10			Glu88(OE2) Asn282(O) His341(CE1)
Total		14		86

significantly stronger than that of entries 6–7 that lack the double bond in the linker.

From the comparison of the inhibition constants, it seems that the double bond confers to potency as does the second amide group in the linker region.

6.3. X-ray crystallography

The pharmacologically relevant target enzyme is the human liver GPa, but our structural studies were performed with the rmGPb due to the ease in growing suitable crystals for protein-inhibitor complexes. The active site is identically conserved in all mammalian GPs [57], indicating that compounds inhibiting muscle GP by binding at this site are likely to inhibit also liver GP and this has been shown in numerous previous studies [36,53,58–61]. *p*-Coumaroyl glucose was found bound at the active site of rmGPb with all atoms well defined within the electron density map (Fig. 2). The binding did not cause any significant conformational changes of the polypeptide chain.

Superposition of the native T state rmGPb structure (PDB entry 7O8E) onto the rmGPb-*p*-coumaroyl glucose complex structure over well-defined residues (18–49, 262–312, 326–829 gave an r.m.s.d. of 0.19 Å and 0.8 Å for the Cα atoms and all residue atoms, respectively. The binding of the glucopyranose ring is very similar to the binding of all glucose derived inhibitors to the active site of rmGPb [2,4,6,14,62] engaging in an extended network of hydrogen bond interactions with residues of the active site (Table 3; Fig. 3).

Atom O2 of the linker (Scheme 1) forms a hydrogen bond interaction with the main chain nitrogen of Leu136 (Table 3 and Fig. 3) and participates to a water mediated interaction with Asp283 OD1, Glu88 OE2, Gly134 N, and Gly137 N. These interactions are reminiscent to the interaction of inhibitors with similar linkers in *N*-acetyl-*β*-D-glucopyranosylamine derivatives [63–70] and promote the closed geometries and give rise to increased rigidity of the 280s and 380s loops. However, in all β-D-glucopyranosylamine and spirohydantoin analogues of β-D-glucopyranose there is a conserved hydrogen bond interaction between the main chain carbonyl oxygen of His377 and the nitrogen atom that has the place of O1′ at the *p*-coumaroyl glucose molecule. This interaction is absent in the *p*-coumaroyl glucose complex and O1′ is 3.8 Å away from the main chain nitrogen of His377. The length of the linker seems to be important in the inhibitory potency of the ligand since ligands with shorter linkers than 4 atoms have 2–3 fold larger K_i values [2,4,6]. The linker of *p*-coumaroyl glucose is also involved in 13 van der Waals interactions with residues Gly135, Leu136, Asp283 and Ans284 (Table 3). The hydroxyphenyl group binds at the so-called β-cavity (a channel lined up with hydrophobic groups adjacent to the active site [4]) engaging in 23 van der Waals interactions. The hydroxyl group O8 forms a hydrogen bond with the main chain carbonyl oxygen of Phe285 and water mediated interactions with Ala383, Arg292, Glu287 and Glu385 (Fig. 3). On

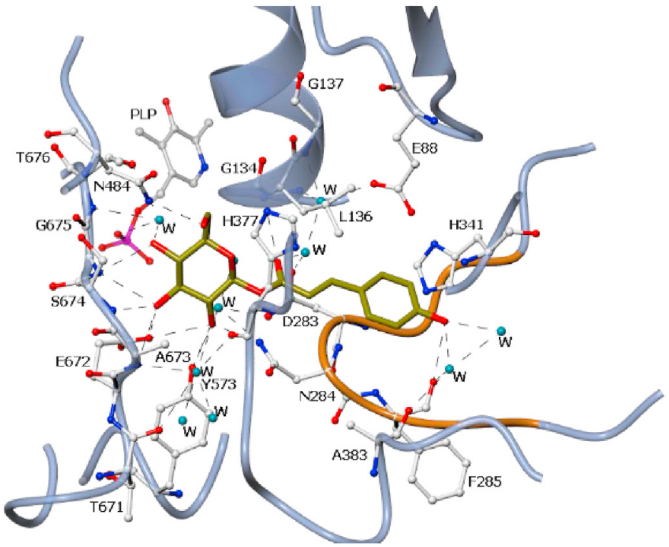

Fig. 3. The binding of *p*-coumaroyl glucose at the rmGPb active site. The inhibitor molecules are shown as thick bonds, water molecules as cyan spheres (labeled W) and hydrogen bond interactions as dashed lines. (For interpretation of the references to colour in this figure legend, the reader is referred to the Web version of this article.)

forming the rmGPb complex *p*-coumaroyl-glucose becomes buried. The solvent accessibilities of the free and bound ligand molecule are 571 and 19 Å^2, respectively, indicating that ~96% of the inhibitor surface becomes buried. On the protein surface, a total of 916 Å^2 solvent accessible surface area becomes inaccessible on binding of the inhibitor.

The closest structurally, to *p*-coumaroyl glucose, GP inhibitors are presented in Table 2. They all have an amide instead of oxygen at the linker component of the glucopyranose inhibitor. Comparative structural analysis of the rmGPb - *p*-coumaroyl glucose complex and the rmGPb in complex with inhibitors in entries **2**–**5** (Table 2) revealed that while all four ligands upon binding induce a significant conformational change of the 280s loop, *p*-coumaroyl-glucose does not (Fig. 4). The r.m.s. distance for residues 281–288, between the GPb - *p*-coumaroyl glucose structure and the GPb in complex with inhibitors 2–5 (Table 2) is 2.3, 2.2, 1.5, and 2.1 Å, respectively. The 280s conformational change was attributed to the presence of the bulky phenyl substituent which induced a significant movement of this loop away from the active site to make space for the inhibitor [54].

Comparing the protein interactions of *p*-coumaroyl glucose to those of entries 2–5 in Table 2 reveals that the linker part is involved in similar interactions with protein residues including a hydrogen bond to the main chain amide of Leu136 (Fig. 3). The rest of the atoms of the aromatic group engage in similar van der Waals interactions with protein residues; 23 for *p*-coumaroyl glucose, and 25, 24, 24, and 27 for entries 2, 3, 4, and 5 in Table 2, respectively). Their most significant difference in their interactions is the hydrogen bond of the hydroxyphenyl group of *p*-coumaroyl glucose to the main chain carbonyl oxygen of Phe285. This interaction together with two water mediated hydrogen bond interactions of the O8 hydroxyl group of *p*-coumaroyl glucose to Arg292, Glu385 seem to counterbalance any conformational change might have caused by the binding of the hydrophobic hydroxyphenyl group of the inhibitor. Interestingly, although inhibitor of entry 2 in Table 2 has a hydroxyphenyl group induces the conformational change of the 280s loop and its hydroxyl group is 5.7 Å away from the main chain carbonyl oxygen of Phe285. The new conformation of the 280s loop is stabilized by a water mediated hydrogen bond with the second carbonyl oxygen of the linker to Asp283, a bond which *p*-coumaroyl glucose cannot form since it lacks this group. Thus, the 280s conformational change is not caused solely by the hydrophobicity or the bulkiness of the inhibitor but it also depends on whether it will find suitable interactions to stabilize in the new adopted conformation. The inhibitory potency of *p*-coumaroyl glucose is 3.8–6.8 times smaller than that of entries 2–5. This may be attributed to the failure of *p*-coumaroyl glucose to induce the conformational change of the 280s loop. This change causes a 180° flip of Asn284 which is positioned between the phenyl rings of Phe285 and Tyr613, two residues that constitute the inhibitor site at the entrance of the catalytic site in GPb, resulting in its blockage. This rearrangement of the 280 s loop is in the direction of the R to T allosteric transition, causing the destruction of the GPb inhibitor site and changes at the intersubunit contacts of the dimer which give rise to allosteric effects [71]. It has been also observed in other GPb ligand complexes with bulky benzoyl moieties that bind at the active site [2,54] Thus, *p*-coumaroyl-glucose is a weaker inhibitor. This further supported by the similar inhibitory potency of compound in entry 1 in Table 2, which lacks the hydroxyl group O8 (Scheme 1) of *p*-coumaroyl glucose. In the absence of the crystal structure of the rmGPb-1 complex we assume that the phenyl substituent causes a less extensive or no conformational change of the 280s loop, than the rest of the inhibitors.

6.4. ^{1}H NMR based metabolomics analysis

Cell medium and cell extracts, in the presence and absence of *p*-coumaroyl glucose from three different flasks were screened (12 samples). For each biofluid, the corresponding "chemical environment" (DMEM, DMEM with glucagon, and the cell lysis buffer) was also analyzed. Typical ^{1}H 1D Noesy presat NMR spectra of cell extracts and

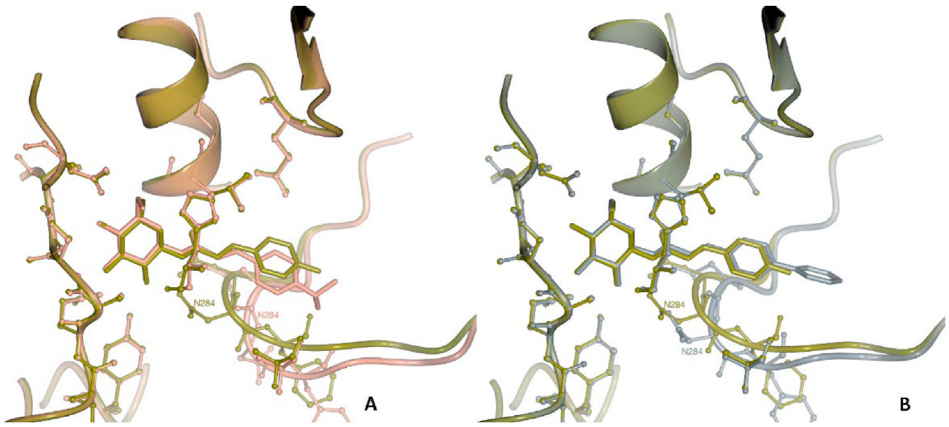

Fig. 4. Superposition of the rmGPb-*p*-coumaroyl glucose complex structure (gold) onto the structure of the rmGPb-**4** complex in pink (A) and onto the rmGPb-**5** complex in grey (B). Asn284 is labeled in each of the complexes. (For interpretation of the references to colour in this figure legend, the reader is referred to the Web version of this article.)

Table 4
Fold change results of the identified and assigned metabolites in the two biological samples.

Metabolites of cell extract	Fold change[a]	Metabolites of cell media	Fold change[b]
Acetate	0.202	Ethanol	0.142
Creatine	−0.13	Creatinine	0.123
Lactate	*	Lactate	0.51
Alanine	−2.555	Alanine	0.181
Isoleucine	0.059	Lysine	0.025
Glutamate	−0.131	Valine	0.005
Glycine	−0.247	Isoleucine	0.037
Leucine	0.761	Leucine	0.041
Glutamine	−0.432	Pyroglutamate	0.009
O-phosphocholine	−0.123	Glutamine	0.020
Valine	−0.248	Myo-inositol	1.736
Threonine	*	Methanol	0.817
Choline	−0.733	Formate	0.277
$NAD^{+/}$NADH	−0.294	Phenylalanine	−0.021
UDP-galactose	1.523	Tyrosine	0.024
UDP-glucuronate	−0.621	Maltose	*
Uridine	inf	Tryptophan	−0.081
EDTA	*	Homoserine	*
Mannitol	−0.201	Niacinamide?	*
Unsaturated fatty acids	−0.526	Cadaverine	0.024
Fatty acid Alkyl chain $-(CH_2)_n$-	−0.321		
Glycylproline	*	Dimethylamine	−0.084
Carnitine	−0.276	Homocysteine	0.261
N-acetyl glutamate	*	*N*-acetylglucosamine	*
Isopropanol	−0.241	Glucuronate	*
AMP	-inf	Arginine	−0.035
UMP	−0.026	Glycerol-derivatives	*
Acetone/acetoin	-.0258	1-Methylhistidine	0.087
Oxypurinol	0.84	Ketoleucine	−0.183
2-deoxyadenosine	inf	Nicotinurate	−0.102
N-Nitrosodimethylamine	0.109	5-aminolevulinic acid	*
Methanol	1.116	Sn-*glycero*-3-phosphocholine	0.114
methylamine	0.077		

[a] Metabolite's fold changes are presented using the calculated metabolite peak area in NMR spectra of control and *p*-coumaroyl cell extracts (Δp-coumaroyl glucose/control); [b] Metabolite's fold changes are presented using the calculated metabolite peak area in NMR spectra of control and *p*-coumaroyl glucose cell media (Δp-coumaroyl glucose/control); * metabolites not subjected to univariate analysis due to ^{1}H overlapped signals.

cell media samples were obtained from the sets of different cell culture conditions. Analysis and assignment of ^{1}H NMR spectra contributed significantly to the identification of the metabolites (summarized in Table 4), whose contribution dictates the clustering trends and are valuable to enhance the accuracy of the classification presented below. The two biological fluids were analyzed, and their results were evaluated distinctively since the metabolic inference is based on the *endo*- and the *exo* – HepG2 cells metabolic activity. The data obtained by the bucketing of the twelve spectra were first explored by principal component analysis (data not shown), whilst the clustering was achieved by using the PLS-DA model. PLS-DA models were validated using Leave One Out Cross Validation (LOOCV) method. This analysis revealed for the cell extracts dataset an accuracy of 66.6% (R2: 99%, Q2: −12%) (Fig. 5), while for the cell medium dataset the PLS-DA model exhibited an accuracy of 50%, (R2: 99.9%, Q2: −100%) (Fig. 6).

Multivariate analysis of the two biological fluids reveals metabolites arising in highly overlapped NMR spectral regions. More specifically, comparison of *cell extracts* metabolic profile reveals significantly decreased levels of threonine, choline, *N*-acetylaspartate, leucine and lipids in the presence of *p*-coumaroyl glucose. Similarly, comparison of the *cell medium* metabolic profiles indicated higher levels of proline, 5-aminolevulinate, 1-methylhistidine, sugars (highly overlapped sugar backbone spectral area δ_H:3.00–4.00 ppm), *N*-acetylglucosamine, sn-glycerol-3-phosphocholine, glycerol derivatives, glutamine and glutathione in *p*-coumaroyl glucose treated cells.

Additionally, the presence of *p*-coumaroyl glucose in cell media seem to significantly contribute (*p*-coumaroyl glucose ^{1}H signals arising from the protons presented in Table S1) in clustering (VIP scores, Fig. 6). Biochemical composition of cell medium is representative of the dynamic metabolic process of the cultured cells. Hence, cell medium metabolites manifest a vast number of metabolites, which qualitatively can be attributed to both cellular excretion but also to the essential nutrients derived from their selected nutritional environment, herein the Dulbecco's modified Eagles Medium (DMEM, high glucose). Cell medium metabolomic data presented in this study exhibit the complexity of the biofluid's nature. However, it should be stressed out that metabolic profiling results are greatly depended on cultured media selection. NMR analysis of the DMEM's metabolite composition does not correlate with the cell media metabolism of the two examined groups.

6.5. Pathway analysis

To identify the most relevant metabolic pathways involved in *p*-coumaroyl glucose addition in HepG2 cells, univariate analysis data were subjected in pathway analysis using MetaboAnalyst 5.0. Analysis conducted using the compound list, result of the semiquantitative data for each sample group, cell extracts and cell media. The lists were as uploaded and processed using the *homo sapiens* library from KEGG public database (https://www.genome.jp/kegg/kegg.html). Pathway topology

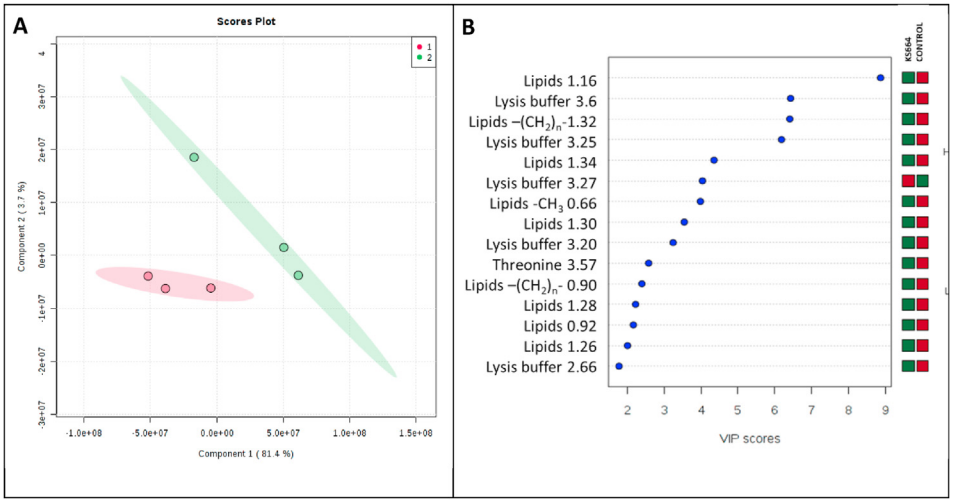

Fig. 5. Multivariate analysis of 1D ^{1}H NOESY cell extracts spectra of the control and the *p*-coumaroyl glucose group. (A) Partial Least Squares-Discriminant Analysis (PLS-DA) 2D scores plot; control group is represented by green spheres and the *p*-coumaroyl-glucose group by red spheres. (B) Important features identified by PLS-DA -variable importance in projection (VIP) scores. The colored boxes on the right indicate the relative concentrations of the corresponding metabolite in each group under study. The dataset was mean centered. (For interpretation of the references to colour in this figure legend, the reader is referred to the Web version of this article.)

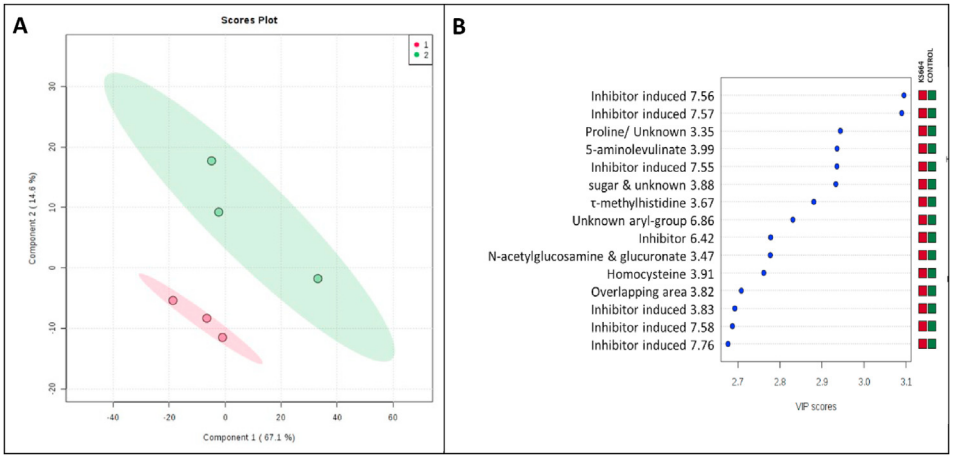

Fig. 6. Multivariate analysis of 1D ^{1}H NOESY cell medium spectra of the control and *p*-coumaroyl glucose group. (A) PLS-DA 2D scores plot; control group is represented by green spheres and the *p*-coumaroyl glucose group by red spheres. (B) Important features identified by PLS-DA -variable importance in projection (VIP) scores. The colored boxes on the right indicate the relative concentrations of the corresponding metabolite in each group under study. The dataset was normalized by sum and autoscaled. (For interpretation of the references to colour in this figure legend, the reader is referred to the Web version of this article.)

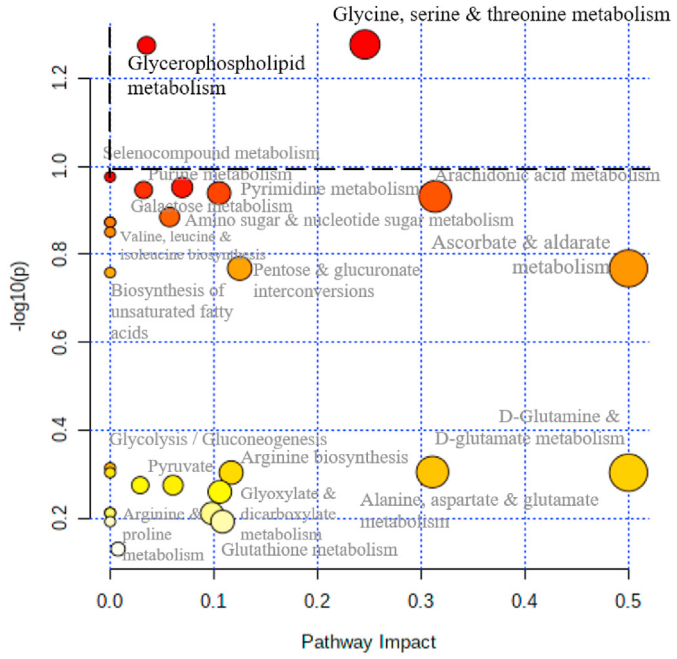

Fig. 7. Pathway analysis of cell extracts NMR metabolomic data displaying metabolic pathways arranged by scores from pathway enrichment analysis (y axis) and from topology analysis (x axis). Each point represents a metabolic pathway. The colour and the size of each circle is based on p-values and pathway impact values, respectively. (For interpretation of the references to colour in this figure legend, the reader is referred to the Web version of this article.)

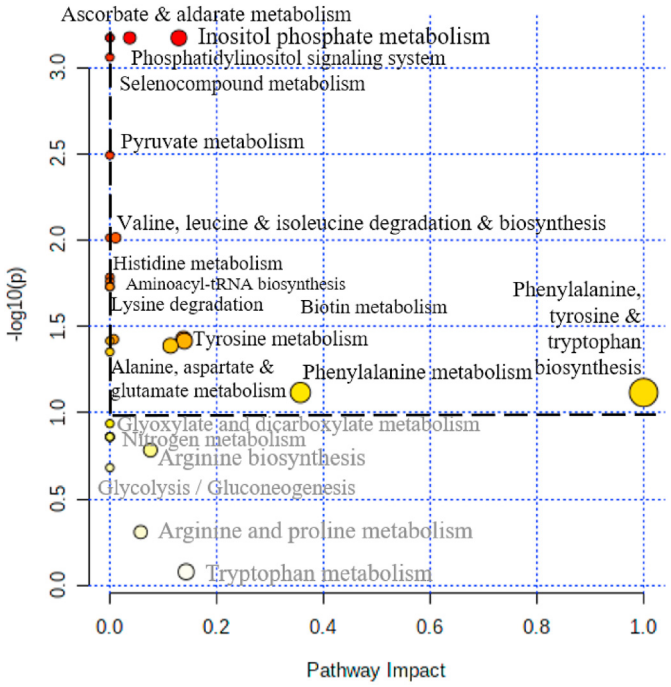

Fig. 8. Pathway analysis of cell media NMR metabolomic data displaying metabolic pathways arranged by scores from pathway enrichment analysis (y axis) and from topology analysis (x axis). Each point represents a metabolic pathway. The colour and the size of each circle is based on p-values and pathway impact values, respectively. (For interpretation of the references to colour in this figure legend, the reader is referred to the Web version of this article.)

analysis revealed the impact values for each active metabolic pathway. P values were calculated from the metabolite set enrichment analysis (Tables S2 and S3). Each dot point represents one metabolic pathway, while the size of the dot correlates positively with the impact of the pathway in each dataset.

The highly differential metabolites of cell extracts indicate the pathways of Glycine, serine, and threonine metabolism (p. value 0.0529) and Glycerophospholipid metabolism (p. values 0.0531) as the most altered pathways upon *p*-coumaroyl glucose treatment. Observation of the decreased levels of choline and creatine and the moderate higher levels of glycine in *p*-coumaroyl glucose group respect to control group, suggest that Glycine, serine, and threonine metabolic pathway is the most significantly involved biochemical pathway. Whilst elevated levels of choline phosphate and decreased levels of choline in *p*-coumaroyl glucose group contribute to the significance of the glycerophospholipid pathway (Fig. 7). However, the pathways with the greater impact regarding cell extracts are ascorbate and aldarate metabolism (impact: 0.5), D-glutamine and D-glutamate metabolism (impact: 0.5), arachidonic acid metabolism (impact: 0.3135), alanine, aspartate and glutamate metabolism (impact: 0.3109), glycine, serine and threonine metabolism (impact: 0.24577), pyrimidine metabolism (impact: 0.10507) and pentose and glucuronate interconversions (impact: 0.125).

In addition, some relatively low impact pathways involve more than three statistically significant changed metabolites. These include choline which implicates glycine, serine & threonine and glycerophospholipid metabolism. Creatine and L-glutamine indicating the purine metabolism, UDP-α-galactose levels designate the galactose metabolism, and alanine levels demonstrating the selenocompound metabolism (Fig. 7).

Cell media metabolites are mostly indicating the myoinositol metabolism. Elevated levels of myoinositol in cell medium samples of the *p*-coumaroyl glucose treated cells suggests that inositol phosphate, galactose metabolism (p. value 6.7597E-4), phosphatidylinositol signaling system (p. value 6.7597E-4) and ascorbate and aldarate metabolism (p. value 6.7597E-4) are highly triggered. Also increased levels of Alanine in *p*-coumaroyl glucose treated cell media, indicate the involvement of selenocompound metabolism (p. value 8.7488E-4). High levels of excreted lactate in *p*-coumaroyl glucose treated cells suggest stimulation of the pyruvate metabolism (p. value 0.0032). Furthermore, increased levels of branched chain amino acids (BCAAs) underlying an increase in valine, leucine, and isoleucine metabolism activation (p. value 0.0097269). Cell medium pathways of high impact but not of the same statistical significance are three. The phenylalanine, tyrosine, and tryptophan biosynthesis pathway (impact: 1.0), phenylalanine metabolism (impact: 0.357) and tyrosine metabolism (impact: 0.14) (Fig. 8). These results may be attributed to the culture medium used, since DMEM contains high amounts of isoleucine, leucine, valine, glycine, choline, phenylalanine, and tyrosine.

The analysis of the metabolic profile of the HepG2 cells indicates a decrease in the concentration levels of certain metabolites, in the presence of *p*-coumaroyl glucose, in the cell extracts. These metabolites are threonine, mannitol, choline, unsaturated lipids ω-3/6, saturated lipids, and *N*-acetylaspartate. Reduced threonine levels could explain the increase towards glycine and acetate percentages. Increased levels of methylamine in HepG2 cells could be a notification of a more active glucose uptake process, in agreement with studies on the regulation of glucose transportation in human adipocytes [72,73]. Furthermore, reduction of choline, which serves as essential nutrient and is a component of the phosphocholine membrane phospholipid, may be indicative of the fatty acid decreased levels in HepG2 cells. This fact, along with the increase of acetate levels after *p*-coumaroyl glucose treatment suggest enhanced fatty acid oxidation [74]. Elevated leucine and isoleucine levels induced by the presence of *p*-coumaroyl glucose indicate lack of any BCAAs deficiency, regulating thus HepG2 cells hepatic fatty acid synthesis, transport, oxidation, and lipolysis. Increased hepatic fatty acid oxidation could act as an alternative pathway for energy production upon glycogen metabolism inhibition. BCAAs are known as activators of mTOR signaling pathway hence promoting insulin resistance through the serine phosphorylation of insulin receptor proteins and increasing protein synthesis [75,76]. Thus, leucine and isoleucine levels could be an additional indicator of *p*-coumaroyl glucose response mechanism in regulation of insulin resistance. Additionally, the presence of *p*-coumaroyl glucose also differentiates the levels of metabolites found in the cell media regarding mainly saccharides, glycerol derivatives and amino acids. Specifically, myoinositol, lactate, and alanine are found decreased in the cell media of the control samples, while the levels of glycerol conjugated metabolites as sn-glycerol-3-phosphate and sn-glycerol-3-phosphocholine, proline, 5-oxoproline, glutamine and glutathione are found increased in the *p*-coumaroyl glucose treated cells. The increase of myoinositol in cell medium upon *p*-coumaroyl glucose addition is indicative of the cells' active response to higher glucose cell uptake from their environment (medium), in combination with the possible ‘‘insulin-sensitizing’’ effect, that *p*-coumaroyl glucose induce and may lead to impaired extracellular myoinositol uptake [77,78]. In addition, elevated lactate, and alanine levels in cell media of *p*-coumaroyl glucose supports further the enhanced gluconeogenesis towards lipid metabolism and glycerol-derived components' accumulation in the media. This is the first time where the effect of a GP inhibitor in the hepatic cellular metabolome is examined and as such it will have significant implications on future rational GP-inhibitor design studies.

Acknowledgments

This research is co-financed by Greece and the European Union (European Social Fund- ESF) through the Operational Programme « Human Resources Development, Education and Lifelong Learning 2014–2020» in the context of the project “Structure guided design of glycogenolysis regulators to develop new therapeutic agents (MIS 5048932)”. Synthetic work was supported by the National Research, Development and Innovation Office of Hungary (Grant FK132222) and the EU co-financed by the European Regional Development Fund under Project GINOP-2.3.2-15-2016-00008.

Appendix A. Supplementary data

Supplementary data to this article can be found online at https://doi.org/10.1016/j.ejmcr.2021.100011.

References

[1] G.A. Stravodimos, B.A. Chetter, E. Kyriakis, A.L. Kantsadi, D.S. Chatzileontiadou, V.T. Skamnaki, A. Kato, J.M. Hayes, D.D. Leonidas, Phytogenic polyphenols as glycogen phosphorylase inhibitors: the potential of triterpenes and flavonoids for glycaemic control in type 2 diabetes, Curr. Med. Chem. 24 (2017) 384–403.
[2] L. Somsak, K. Czifrak, M. Toth, E. Bokor, E.D. Chrysina, K.M. Alexacou, J.M. Hayes, C. Tiraidis, E. Lazoura, D.D. Leonidas, S.E. Zographos, N.G. Oikonomakos, New inhibitors of glycogen phosphorylase as potential antidiabetic agents, Curr. Med. Chem. 15 (2008) 2933–2983.
[3] T. Docsa, K. Czifrak, C. Huse, L. Somsak, P. Gergely, Effect of glucopyranosylidene-spiro-thiohydantoin on glycogen metabolism in liver tissues of streptozotocin-induced and obese diabetic rats, Mol. Med. Rep. 4 (2011) 477–481.
[4] N.G. Oikonomakos, Glycogen phosphorylase as a molecular target for type 2 diabetes therapy, Curr. Protein Pept. Sci. 3 (2002) 561–586.
[5] L. Somsák, E. Bokor, K. Czifrák, L. Juhász, M. Tóth, Carbohydrate derivatives and glycomimetic compounds in established and investigational therapies of type 2 diabetes mellitus, in: M. Zimering (Ed.), Topics in the Prevention, Treatment and Complications of Type 2 Diabetes, InTech, 2011.
[6] L. Somsak, Glucose derived inhibitors of glycogen phosphorylase, Compt, Rend. Chim. 14 (2011) 211–223.
[7] T. Docsa, B. Marics, J. Nemeth, C. Huse, L. Somsak, P. Gergely, B. Peitl, Insulin sensitivity is modified by a glycogen phosphorylase inhibitor: glucopyranosylidene-spiro-thiohydantoin in streptozotocin-induced diabetic rats, Curr. Top. Med. Chem. 15 (2015) 2390–2394.
[8] D. Goyard, B. Konya, A.S. Chajistamatiou, E.D. Chrysina, J. Leroy, S. Balzarin, M. Tournier, D. Tousch, P. Petit, C. Duret, P. Maurel, L. Somsak, T. Docsa, P. Gergely, J.P. Praly, J. Azay-Milhau, S. Vidal, Glucose-derived spiro-isoxazolines are anti-hyperglycemic agents against type 2 diabetes through glycogen phosphorylase inhibition, Eur. J. Med. Chem. 108 (2016) 444–454.
[9] L. Nagy, J. Marton, A. Vida, G. Kis, E. Bokor, S. Kun, M. Gonczi, T. Docsa, A. Toth, M. Antal, P. Gergely, B. Csoka, P. Pacher, L. Somsak, P. Bai, Glycogen phosphorylase inhibition improves beta cell function, Br. J. Pharmacol. 175 (2018) 301–319.
[10] C.E. Zois, A.L. Harris, Glycogen metabolism has a key role in the cancer microenvironment and provides new targets for cancer therapy, J. Mol. Med. 94 (2016) 137–154.
[11] L. Xu, H. Sun, Pharmacological manipulation of brain glycogenolysis as a therapeutic approach to cerebral ischemia, Mini Rev. Med. Chem. 10 (2010) 1188–1193.
[12] T. Guan, Y.S. Qian, X.Z. Tang, M.H. Huang, L.F. Huang, Y.M. Li, H.B. Sun, Maslinic acid, a natural inhibitor of glycogen phosphorylase, reduces cerebral ischemic injury in hyperglycemic rats by GLT-1 up-regulation, J. Neurosci. Res. 89 (2011) 1829–1839.
[13] A. Sipos, E. Szennyes, N.E. Hajnal, S. Kun, K.E. Szabo, K. Uray, L. Somsak, T. Docsa, E. Bokor, Dual-target compounds against type 2 diabetes mellitus: proof of concept for sodium dependent glucose transporter (SGLT) and glycogen phosphorylase (GP) inhibitors, Pharmaceuticals 14 (2021).
[14] J.M. Hayes, A.L. Kantsadi, D.D. Leonidas, Natural products and their derivatives as inhibitors of glycogen phosphorylase: potential treatment for type 2 diabetes, Phytochemistry Rev. 13 (2014) 471–498.
[15] D. Barford, S.H. Hu, L.N. Johnson, Structural mechanism for glycogen phosphorylase control by phosphorylation and AMP, J. Mol. Biol. 218 (1991) 233–260.
[16] D. Barford, L.N. Johnson, The allosteric transition of glycogen phosphorylase, Nature 340 (1989) 609–616.
[17] E. Kyriakis, G.A. Stravodimos, A.L. Kantsadi, D.S. Chatzileontiadou, V.T. Skamnaki, D.D. Leonidas, Natural flavonoids as antidiabetic agents. The binding of gallic and ellagic acids to glycogen phosphorylase b, FEBS Lett. 589 (2015) 1787–1794.
[18] C.E. Drakou, C. Gardeli, I. Tsialtas, S. Alexopoulos, A. Mallouchos, S.M. Koulas, A.S. Tsagkarakou, D. Asimakopoulos, D.D. Leonidas, A.G. Psarra, V.T. Skamnaki, Affinity crystallography reveals binding of pomegranate juice anthocyanins at the inhibitor site of glycogen phosphorylase: the contribution of a sugar moiety to potency and its implications to the binding mode, J. Agric. Food Chem. 68 (2020) 10191–10199.
[19] G.A. Stravodimos, A.L. Kantsadi, A. Apostolou, E. Kyriakis, V.N. Kafaski-Kanelli, T. Solovou, P. Gatzona, P.G.V. Liggri, S. Theofanous, V.A. Gorgogietas, A. Kissa, C. Psachoula, A. Lemonakis, D.S.M. Chatzileontiadou, A.G. Psarra, V.T. Skamnaki, S.A. Haroutounian, D.D. Leonidas, Affinity crystallography reveals the bioactive

compounds of industrial juicing byproducts of punica granatum for glycogen phosphorylase, Curr. Drug Discov. Technol. 15 (2018) 41–53.
[20] X. Wen, H. Sun, J. Liu, K. Cheng, P. Zhang, L. Zhang, J. Hao, P. Ni, S.E. Zographos, D.D. Leonidas, K.M. Alexacou, T. Gimisis, J.M. Hayes, N.G. Oikonomakos, Naturally occurring pentacyclic triterpenes as inhibitors of glycogen phosphorylase: synthesis, structure-activity relationships, and X-ray crystallographic studies, J. Med. Chem. 51 (2008) 3540–3554.
[21] N.G. Oikonomakos, C. Tiraidis, D.D. Leonidas, S.E. Zographos, M. Kristiansen, C.U. Jessen, L. Norskov-Lauritsen, L. Agius, Iminosugars as potential inhibitors of glycogenolysis: structural insights into the molecular basis of glycogen phosphorylase inhibition, J. Med. Chem. 49 (2006) 5687–5701.
[22] K.E. Tsitsanou, J.M. Hayes, M. Keramioti, M. Mamais, N.G. Oikonomakos, A. Kato, D.D. Leonidas, S.E. Zographos, Sourcing the affinity of flavonoids for the glycogen phosphorylase inhibitor site via crystallography, kinetics and QM/MM-PBSA binding studies: comparison of chrysin and flavopiridol, Food Chem. Toxicol. 61 (2013) 14–27.
[23] K. Pei, J. Ou, J. Huang, S. Ou, p-Coumaric acid and its conjugates: dietary sources, pharmacokinetic properties and biological activities, J. Sci. Food Agric. 96 (2016) 2952–2962.
[24] S. Adisakwattana, K. Sookkongwaree, S. Roengsumran, A. Petsom, N. Ngamrojnavanich, W. Chavasiri, S. Deesamer, S. Yibchok-anun, Structure-activity relationships of trans-cinnamic acid derivatives on alpha-glucosidase inhibition, Bioorg. Med. Chem. Lett 14 (2004) 2893–2896.
[25] S. Chethan, S.M. Dharmesh, N.G. Malleshi, Inhibition of aldose reductase from cataracted eye lenses by finger millet (Eleusine coracana) polyphenols, Bioorg. Med. Chem. 16 (2008) 10085–10090.
[26] D. Liang, Y.F. Liu, Z.Y. Hao, H. Luo, Y. Wang, C.L. Zhang, R.Y. Chen, D.Q. Yu, Acylated flavonol glycosides and delta-truxinate derivative from the aerial parts of Lysimachia clethroides, Phytochemistry Letters 11 (2015) 116–119.
[27] S.A. Yoon, S.I. Kang, H.S. Shin, S.W. Kang, J.H. Kim, H.C. Ko, S.J. Kim, p-Coumaric acid modulates glucose and lipid metabolism via AMP-activated protein kinase in L6 skeletal muscle cells, Biochem. Biophys. Res. Commun. 432 (2013) 553–557.
[28] A. Kato, Y. Minoshima, J. Yamamoto, I. Adachi, A.A. Watson, R.J. Nash, Protective effects of dietary chamomile tea on diabetic complications, J. Agric. Food Chem. 56 (2008) 8206–8211.
[29] M. Rafraf, M. Zemestani, M. Asghari-Jafarabadi, Effectiveness of chamomile tea on glycemic control and serum lipid profile in patients with type 2 diabetes, J. Endocrinol. Invest. 38 (2015) 163–170.
[30] M. Zemestani, M. Rafraf, M. Asghari-Jafarabadi, Chamomile tea improves glycemic indices and antioxidants status in patients with type 2 diabetes mellitus, Nutrition 32 (2016) 66–72.
[31] J.A. Villa-Rodriguez, E. Aydin, J.S. Gauer, A. Pyner, G. Williamson, A. Kerimi, Green and chamomile teas, but not acarbose, attenuate glucose and fructose transport via inhibition of GLUT2 and GLUT5, Mol. Nutr. Food Res. 61 (2017).
[32] Y.M. Zhu, J. Ralph, Stereoselective synthesis of 1-O-beta-feruloyl and 1-O-beta-sinapoyl glucopyranoses, Tetrahedron Lett. 52 (2011) 3729–3731.
[33] T. Ziegler, G. Pantkowski, Preparation of 1-O-Acyl-D-Glycopyranoses via chloroacetylated glycopyranosyl donors, J. Carbohydr. Chem. 12 (1993) 357–370.
[34] J.L. Hixson, Y. Hayasaka, C.D. Curtin, M.A. Sefton, D.K. Taylor, Hydroxycinnamoyl glucose and tartrate esters and their role in the formation of ethylphenols in wine, J. Agric. Food Chem. 64 (2016) 9401–9411.
[35] B. Baderschneider, P. Winterhalter, Isolation and characterization of novel benzoates, cinnamates, flavonoids, and lignans from riesling wine and screening for antioxidant activity, J. Agric. Food Chem. 49 (2001) 2788–2798.
[36] E. Kyriakis, T.G.A. Solovou, S. Kun, K. Czifrak, B. Szocs, L. Juhasz, E. Bokor, G.A. Stravodimos, A.L. Kantsadi, D.S.M. Chatzileontiadou, V.T. Skamnaki, L. Somsak, D.D. Leonidas, Probing the beta-pocket of the active site of human liver glycogen phosphorylase with 3-(C-beta-D-glucopyranosyl)-5-(4-substituted-phenyl)-1, 2, 4-triazole inhibitors, Bioorg. Chem. 77 (2018) 485–493.
[37] T. Fischer, S.M. Koulas, A.S. Tsagkarakou, E. Kyriakis, G.A. Stravodimos, V.T. Skamnaki, P.G.V. Liggri, S.E. Zographos, R. Riedl, D.D. Leonidas, High consistency of structure-based design and X-ray crystallography: design, synthesis, kinetic evaluation and crystallographic binding mode determination of biphenyl-N-acyl-beta-D-glucopyranosylamines as glycogen phosphorylase inhibitors, Molecules 24 (2019) 1322.
[38] R.J. Leatherbarrow, GraFit Version 6.0, Erithakus Software, Staines, UK, 2007.
[39] W. Kabsch, XDS, Acta Crystallogr. D Biol. Crystallogr. 66 (2010) 125–132.
[40] CCP4, The CCP4 suite : programs for protein crystallography, Acta Crystallogr. D 50 (1994) 760–763.
[41] G.N. Murshudov, P. Skubak, A.A. Lebedev, N.S. Pannu, R.A. Steiner, R.A. Nicholls, M.D. Winn, F. Long, A.A. Vagin, REFMAC5 for the refinement of macromolecular crystal structures, Acta Crystallogr. D Biol. Crystallogr. 67 (2011) 355–367.
[42] D.D. Leonidas, S.E. Zographos, K.E. Tsitsanou, V.T. Skamnaki, G. Stravodimos, E. Kyriakis, Glycogen phosphorylase revisited: extending the resolution of the R- and T-state structures of the free enzyme and in complex with allosteric activators, Acta Crystallogr. F77 (2021) 303–311.
[43] A.A. Lebedev, P. Young, M.N. Isupov, O.V. Moroz, A.A. Vagin, G.N. Murshudov, JLigand: a graphical tool for the CCP4 template-restraint library, Acta Crystallogr, D Biol. Crystallogr. 68 (2012) 431–440.
[44] R.P. Joosten, F. Long, G.N. Murshudov, A. Perrakis, The PDB_REDO server for macromolecular structure model optimization, I.U.Cr.J. 1 (2014) 213–220.
[45] V.B. Chen, W.B. Arendall 3rd, J.J. Headd, D.A. Keedy, R.M. Immormino, G.J. Kapral, L.W. Murray, J.S. Richardson, D.C. Richardson, MolProbity: all-atom structure validation for macromolecular crystallography, Acta Crystallogr. D Biol. Crystallogr. 66 (2010) 12–21.
[46] M.D. Winn, C.C. Ballard, K.D. Cowtan, E.J. Dodson, P. Emsley, P.R. Evans, R.M. Keegan, E.B. Krissinel, A.G. Leslie, A. McCoy, S.J. McNicholas, G.N. Murshudov, N.S. Pannu, E.A. Potterton, H.R. Powell, R.J. Read, A. Vagin, K.S. Wilson, Overview of the CCP4 suite and current developments, Acta Crystallogr. D Biol. Crystallogr. 67 (2011) 235–242.
[47] S.J. Hubbard, J.M. Thornton, NACCESS, Department of Biochemistry and Molecular Biology, University College, London, 1993.
[48] S. McNicholas, E. Potterton, K.S. Wilson, M.E. Noble, Presenting your structures: the CCP4mg molecular-graphics software, Acta Crystallogr. D Biol. Crystallogr. 67 (2011) 386–394.
[49] J. Chong, D.S. Wishart, J. Xia, Using MetaboAnalyst 4.0 for comprehensive and integrative metabolomics data analysis, Curr Protoc Bioinformatics 68 (2019) e86.
[50] H. Katsuragi, K. Shimoda, R. Yamamoto, K. Ishihara, H. Hamada, Glycosylation of capsaicin derivatives and phenylpropanoid derivatives using cultured plant cells, Biochem. Insights 4 (2011). BCI.S6682.
[51] N.G. Oikonomakos, M. Kontou, S.E. Zographos, H.S. Tsitoura, L.N. Johnson, K.A. Watson, E.P. Mitchell, G.W.J. Fleet, J.C. Son, C.J.F. Bichard, D.D. Leonidas, K.R. Acharya, The design of potential antidiabetic drugs: experimental investigation of a number of beta-D-glucose analogue inhibitors of glycogen phosphorylase, Eur. J. Drug Metabol. Pharmacokinet. 19 (1994) 185–192.
[52] S.R. Sprang, E.J. Goldsmith, R.J. Fletterick, S.G. Withers, N.B. Madsen, Catalytic site of glycogen phosphorylase: structure of the T state and specificity for alpha-D-glucose, Biochemistry 21 (1982) 5364–5371.
[53] A.L. Kantsadi, E. Bokor, S. Kun, G.A. Stravodimos, D.S. Chatzileontiadou, D.D. Leonidas, E. Juhasz-Toth, A. Szakacs, G. Batta, T. Docsa, P. Gergely, L. Somsak, Synthetic, enzyme kinetic, and protein crystallographic studies of C-beta-D-glucopyranosyl pyrroles and imidazoles reveal and explain low nanomolar inhibition of human liver glycogen phosphorylase, Eur. J. Med. Chem. 123 (2016) 737–745.
[54] V. Parmenopoulou, A.L. Kantsadi, V.G. Tsirkone, D.S.M. Chatzileontiadou, S. Manta, S.E. Zographos, C. Molfeta, G. Archontis, L. Agius, J.M. Hayes, D.D. Leonidas, D. Komiotis, Structure based inhibitor design targeting glycogen phosphorylase b. Virtual screening, synthesis, biochemical and biological assessment of novel N-acyl-beta-D-glucopyranosylamines, Biorg. Med. Chem. 22 (2014) 4810–4825.
[55] Z. Gyorgydeak, Z. Hadady, N. Felfoldi, A. Krakomperger, V. Nagy, M. Toth, A. Brunyanszki, T. Docsa, P. Gergely, L. Somsak, Synthesis of N-(beta-D-glucopyranosyl)- and N-(2-acetamido-2-deoxy-beta-D-glucopyranosyl) amides as inhibitors of glycogen phosphorylase, Bioorg. Med. Chem. 12 (2004) 4861–4870.
[56] N.G. Oikonomakos, M. Kosmopoulou, S.E. Zographos, D.D. Leonidas, E.D. Chrysina, L. Somsak, V. Nagy, J.P. Praly, T. Docsa, B. Toth, P. Gergely, Binding of N-acetyl-N '-beta-d-glucopyranosyl urea and N-benzoyl-N '-beta-d-glucopyranosyl urea to glycogen phosphorylase b, Eur. J. Biochem. 269 (2002) 1684–1696.
[57] J.W. Hudson, G.B. Golding, M.M. Crerar, Evolution of allosteric control in glycogen phosphorylase, J. Mol. Biol. 234 (1993) 700–721.
[58] E. Bokor, E. Kyriakis, T.G.A. Solovou, C. Koppany, A.L. Kantsadi, K.E. Szabo, A. Szakacs, G.A. Stravodimos, T. Docsa, V.T. Skamnaki, S.E. Zographos, P. Gergely, D.D. Leonidas, L. Somsak, Nanomolar inhibitors of glycogen phosphorylase based on beta-D-glucosaminyl heterocycles: a combined synthetic, enzyme kinetic, and protein crystallography study, J. Med. Chem. 60 (2017) 9251–9262.
[59] A.L. Kantsadi, G.A. Stravodimos, E. Kyriakis, D.S.M. Chatzileontiadou, T.G.A. Solovou, S. Kun, E. Bokor, L. Somsak, D.D. Leonidas, van der Waals interactions govern C-beta-D-glucopyranosyl triazoles' nM inhibitory potency in human liver glycogen phosphorylase, J. Struct. Biol. 199 (2017) 57–67.
[60] S. Kun, J. Begum, E. Kyriakis, E.C.V. Stamati, T.A. Barkas, E. Szennyes, É. Bokor, K.E. Szabó, G.A. Stravodimos, A. Sipos, T. Docsa, P. Gergely, C. Moffatt, M.S. Patraskaki, M.C. Kokolaki, A. Gkerdi, V.T. Skamnaki, D.D. Leonidas, L. Somsák, J.M. Hayes, A multidisciplinary study of 3-(beta-d-glucopyranosyl)-5-substituted-1,2,4-triazole derivatives as glycogen phosphorylase inhibitors: computation, synthesis, crystallography and kinetics reveal new potent inhibitors, Eur. J. Med. Chem. 147 (2018) 266–278.
[61] T. Fischer, S.M. Koulas, A.S. Tsagkarakou, E. Kyriakis, G.A. Stravodimos, V.T. Skamnaki, P.G.V. Liggri, S.E. Zographos, R. Riedl, D.D. Leonidas, High consistency of structure-based design and X-Ray crystallography: design, synthesis, kinetic evaluation and crystallographic binding mode determination of biphenyl-N-acyl-β-D-glucopyranosylamines as glycogen phosphorylase inhibitors, Molecules 24 (2019) 1322.
[62] E. Kyriakis, A.G. Karra, O. Papaioannou, T. Solovou, V.T. Skamnaki, P.G.V. Liggri, S.E. Zographos, E. Szennyes, E. Bokor, S. Kun, A.G. Psarra, L. Somsak, D.D. Leonidas, The architecture of hydrogen and sulfur sigma-hole interactions explain differences in the inhibitory potency of C-beta-d-glucopyranosyl thiazoles, imidazoles and an N-beta-d glucopyranosyl tetrazole for human liver glycogen phosphorylase and offer new insights to structure-based design, Bioorg. Med. Chem. 28 (2020) 115196.
[63] K.M. Alexacou, J.M. Hayes, C. Tiraidis, S.E. Zographos, D.D. Leonidas, E.D. Chrysina, G. Archontis, N.G. Oikonomakos, J.V. Paul, B. Varghese, D. Loganathan, Crystallographic and computational studies on 4-phenyl-N-(beta-D-glucopyranosyl)-1H-1,2,3-triazole-1-acetamide, an inhibitor of glycogen phosphorylase: comparison with alpha-D-glucose, N-acetyl-beta-D-glucopyranosylamine and N-benzoyl-N'-beta-D-glucopyranosyl urea binding, Proteins 71 (2008) 1307–1323.
[64] E.D. Chrysina, E. Bokor, K.M. Alexacou, M.D. Charavgi, G.N. Oikonomakos, S.E. Zographos, D.D. Leonidas, N.G. Oikonomakos, S. Laszlo, Amide-1,2,3-triazole bioisosterism: the glycogen phosphorylase case, Tetrahedron Asymmetry 20 (2009) 733–740.

[65] T. Hadjiloi, C. Tiraidis, E.D. Chrysina, D.D. Leonidas, N.G. Oikonomakos, P. Tsipos, T. Gimisis, Binding of oxalyl derivatives of beta-d-glucopyranosylamine to muscle glycogen phosphorylase b, Bioorg. Med. Chem. 14 (2006) 3872–3882.
[66] E.I. Petsalakis, E.D. Chrysina, C. Tiraidis, T. Hadjiloi, D.D. Leonidas, N.G. Oikonomakos, U. Aich, B. Varghese, D. Loganathan, Crystallographic studies on N-azidoacetyl-beta-D-glucopyranosylamine, an inhibitor of glycogen phosphorylase: comparison with N-acetyl-beta-D-glucopyranosylamine, Bioorg. Med. Chem. 14 (2006) 5316–5324.
[67] E.D. Chrysina, N.G. Oikonomakos, S.E. Zographos, M.N. Kosmopoulou, N. Bischler, D.D. Leonidas, L. Kovacs, T. Docsa, P. Gergely, L. Somsak, Crystallographic studies on alpha- and beta-D-glucopyranosyl formamide analogues, inhibitors of glycogen phosphorylase, Biocatal. Biotransform. 21 (2003) 233–242.
[68] E.D. Chrysina, M.N. Kosmopoulou, C. Tiraidis, R. Kardakaris, N. Bischler, D.D. Leonidas, Z. Hadady, L. Somsak, T. Docsa, P. Gergely, N.G. Oikonomakos, Kinetic and crystallographic studies on 2-(beta-D-glucopyranosyl)-5-methyl-1, 3, 4-oxadiazole, -benzothiazole, and -benzimidazole, inhibitors of muscle glycogen phosphorylase b. Evidence for a new binding site, Protein Sci. 14 (2005) 873–888.
[69] E.D. Chrysina, M.N. Kosmopoulou, R. Kardakaris, N. Bischler, D.D. Leonidas, T. Kannan, D. Loganathan, N.G. Oikonomakos, Binding of beta-D-glucopyranosyl bismethoxyphosphoramidate to glycogen phosphorylase b: kinetic and crystallographic studies, Bioorg. Med. Chem. 13 (2005) 765–772.
[70] E. Anagnostou, M.N. Kosmopoulou, E.D. Chrysina, D.D. Leonidas, T. Hadjiloi, C. Tiraidis, S.E. Zographos, Z. Gyorgydeak, L. Somsak, T. Docsa, P. Gergely, F.N. Kolisis, N.G. Oikonomakos, Crystallographic studies on two bioisosteric analogues, N-acetyl-beta-D-glucopyranosylamine and N-trifluoroacetyl-beta-D-glucopyranosylamine, potent inhibitors of muscle glycogen phosphorylase, Bioorg. Med. Chem. 14 (2006) 181–189.
[71] L.N. Johnson, Glycogen phosphorylase: control by phosphorylation and allosteric effectors, Faseb. J. 6 (1992) 2274–2282.
[72] C. Carpene, P. Mauriege, N. Boulet, S. Biron, J.L. Grolleau, M.J. Garcia-Barrado, M.C. Iglesias-Osma, Methylamine activates glucose uptake in human adipocytes without overpassing action of insulin or stimulating its secretion in pancreatic islets, Medicines (Basel) (2019) 6.
[73] J. O'Sullivan, M. Unzeta, J. Healy, M.I. O'Sullivan, G. Davey, K.F. Tipton, Semicarbazide-sensitive amine oxidases: enzymes with quite a lot to do, Neurotoxicology 25 (2004) 303–315.
[74] L. Liu, C. Fu, F. Li, Acetate Affects the Process of Lipid Metabolism in Rabbit Liver, Skeletal Muscle and Adipose Tissue, Animals (Basel), 2019, p. 9.
[75] S. Zhang, X. Zeng, M. Ren, X. Mao, S. Qiao, Novel metabolic and physiological functions of branched chain amino acids: a review, J. Anim. Sci. Biotechnol. 8 (2017) 10.
[76] K. Tajiri, Y. Shimizu, Branched-chain amino acids in liver diseases, World J. Gastroenterol. 19 (2013) 7620–7629.
[77] M.L. Croze, C.O. Soulage, Potential role and therapeutic interests of myo-inositol in metabolic diseases, Biochimie 95 (2013) 1811–1827.
[78] H. Cabrera-Cruz, L. Orostica, F. Plaza-Parrochia, I. Torres-Pinto, C. Romero, M. Vega, The insulin-sensitizing mechanism of myo-inositol is associated with AMPK activation and GLUT-4 expression in human endometrial cells exposed to a PCOS environment, Am. J. Physiol. Endocrinol. Metab. 318 (2020) E237–E248.